Fabrication of aluminum–alumina metal matrix composites via cold gas dynamic spraying at low pressure followed by friction stir processing

K.J. Hodder [a], H. Izadi [a], A.G. McDonald [b], A.P. Gerlich [c,*]

[a] Department of Chemical and Materials Engineering, University of Alberta, 7th Floor, Electrical & Computer Engineering Research Facility, Edmonton, Alberta, Canada T6G 2V4
[b] Department of Mechanical Engineering, University of Alberta, 4–9 Mechanical Engineering Building, Edmonton, Alberta, Canada T6G 2G8
[c] Department of Mechanical and Mechatronics Engineering, University of Waterloo, 200 University Avenue West, Waterloo, Ontario, Canada N2L 3G1

ARTICLE INFO

ABSTRACT

Cold gas dynamic spraying at low pressure (1 MPa gage or 150 psig) was used to fabricate Al–Al_2O_3 metal matrix composite (MMC) coatings onto 6061 Al alloy. The powder contained Al powder admixed with $-10 \mu m$ Al_2O_3 in fractions up to 90 wt.%. Scanning electron microscopy (SEM), Vickers micro-hardness testing, and image analysis were conducted to determine the microstructure, properties, and volume fraction of reinforcing particles in the coatings. The coatings were then friction-stir processed (FSP) at tool rotation speeds of 894 or 1723 RPM using a flat cylindrical tool. The Al_2O_3 content and hardness of the final MMC coatings increased with increasing fractions of Al_2O_3 particles in the feedstock powder, resulting in a maximum Al_2O_3 content of 48 wt.% and a hardness of 85 HV of the as-sprayed coating when 90 wt.% Al_2O_3 was used in the feed powder blend. After FSP, the hardness of the MMC increased to a maximum of 137 HV. The as-sprayed coatings contained Al_2O_3 particles that were segregated between the Al particles, and FSP was effective in dispersing these Al_2O_3 particles and decreasing their mean free path. It was suggested that this re-distribution and Al_2O_3 particle size refinement during FSP improved the hardness of the MMC coatings.

1. Introduction

Cold gas dynamic spraying (or simply, cold spraying) has been used for surface modification on a variety of structures in the aircraft and automobile industries. It can be used to apply metal, alloy, or metal matrix composite (MMC) coatings by exposing a substrate to high-velocity particles [1], where deposition is accomplished without melting the stock powder particles. This avoids undesirable phase transformations and minimizes the microstructural changes on the substrate material. Plastic deformation of the particles due to the high impact velocities results in the formation of mechanical and/or metallurgical bonds between the particle and the metallic substrate [2–5]. However, due to the morphology of cold-sprayed particles, gas may be trapped during coating deposition that may lead to the formation of pores. Porosity can have a detrimental effect on coating hardness and suppression of porosity is necessary to increase coating hardness [6,7] and improve mechanical properties.

The mechanical properties of cold-sprayed metal coatings may also be improved by incorporating cermet or ceramic reinforcing particles to produce MMC coatings. In this case, a ductile metal powder is co-deposited with a hard phase such as an oxide or a carbide. Numerous investigators [8–10] have found that the blending of alumina (Al_2O_3) particles with aluminum (Al) powder produced a cold-sprayed Al–Al_2O_3 MMC coating with increased hardness compared to that of pure Al coatings. In particular, Irissou et al. [10] have suggested that the content of Al_2O_3 particles in the final coating is limited to 25 wt.% as the content of Al_2O_3 in the powder blend increases. This may prove problematic as powder waste becomes an issue on the industrial, production scale.

Other studies have expanded the development of cold-sprayed MMC coatings to include those in which the reinforcing and matrix materials are harder than Al_2O_3 or Al. Tungsten carbide (WC)-cobalt coatings have been deposited through use of He- or N_2-based high-pressure cold spray systems [11,12]. It was found that the hard WC particles eroded the previously deposited layers of coating, restricting the coating thickness. However, the advantage is that due to the low operating temperature of the cold spray system, no chemical changes such as WC decarburization occurred and the MMC coating hardness was on the order of that fabricated by high-velocity oxy-fuel (HVOF) spraying. A relationship between cold spray gas pressure and the amount of pores in a metallic coating have been investigated by Lee et al. [13], where it was found that the porosity decreases with increased deposition gas pressures due to peening effects. While higher gas

* Corresponding author. Tel.: +1 519 888 4567x38560; fax: +1 780 492 2881.
E-mail address: agerlich@uwaterloo.ca (A.P. Gerlich).

pressures are desirable for deposition of MMC coatings with harder reinforcing materials and reduction in coating porosity, cold spray systems based on high gas pressures require costly equipment and gases. Therefore, there is a need to develop MMC coatings that have been fabricated from low pressure cold spray systems that are usually less expensive.

Friction-stir processing (FSP) has recently been used as a method for increasing the hardness of thermal-sprayed MMC coatings [14]. FSP is an adaptation of friction stir welding (FSW) in which a rotating tool is plunged into the interface between two materials to be joined together and traversed at a constant rate along the edges to create a solid state joint [15]. This process generates heat by a combination of friction and plastic deformation which softens the material without melting the substrate. This process has been shown to improve the hardness of Al–Al$_2$O$_3$ and cemented carbide (WC-CrC-Ni) MMC coatings that have been deposited using air plasma and HVOF spraying [14,16]. In contrast, combining FSP with cold spraying may also provide a viable method to increase coating performance, since both processes operate below the melting temperature of the material. This may produce superior properties due to the refinement that typically occurs when severe plastic deformation is imposed [17]. However, limited studies have explored friction stir processing of cold-sprayed coatings, in particular, coatings deposited by cold spray units operating at low pressure.

There have been numerous studies on the application of the FSP process to fabricate an MMC directly on the surface of a plate in situ by processing a groove or channel on the plate which is filled with reinforcing particles [18]. However, it remains a challenge to prevent the particles from being ejected out of the groove during FSP, and the distribution of particles is typically non-uniform unless multiple FSP passes are applied to homogenize the microstructure. The present work examines the use of cold spraying to apply an MMC layer onto the plate, allowing the material to adhere well to the surface and facilitating fabrication of a uniform coating microstructure in a single pass.

It should be noted that FSP parameters such as travel and tool rotation speeds can have a significant effect on the material properties of the MMC [19]. This is due to the fact that these parameters have a strong influence on the grain size and dissolution of precipitates in heat treatable alloys, and these microstructural features control the material properties of processed Al alloys. During FSP of composites, the parameters further influence the distribution, morphology, and break-up of particles [20,21]. However, these issues have yet to be examined in MMC coatings applied via cold spraying at low pressure. In addition, the use of a simple cylindrical FSP tool (without a pin) has never been considered, although this may be useful to reduce costs related to severe tool wear during abrasion experienced during processing of MMC materials.

The present study investigates the influence of Al$_2$O$_3$ content on cold-sprayed Al–Al$_2$O$_3$ MMC coatings and the effect of FSP on the material properties and microstructure of the coatings. The deposition efficiency, microstructures, and hardness were quantitatively determined before and after FSP. The objective of the study was to determine the feasibility of depositing an MMC coating with a large fraction (greater than 40 wt.%) of hard reinforcing particles, and exposing the coating samples to FSP using a low cost, simple cylindrical tool.

2. Experimental procedure

Information and schematics concerning the cold spray process used in this study have been published extensively [1,22]. A portable cold spray system operating at low pressure (1 MPa gage or 150 psig maximum) (SST series P, CenterLine, Ltd., Windsor, ON, Canada) was used to accelerate and deposit an Al–Al$_2$O$_3$ powder blend. The commercially pure Al powder (SST-A5001, CenterLine, Ltd., Windsor, ON, Canada) had an irregular morphology and the Al$_2$O$_3$ powder (4001155, Almatis, Leetsdale, PA, USA) was sieved to $-10\,\mu$m. The nozzle of the cold spray unit was made of stainless steel with a 6.4 mm exit diameter and 120 mm length. The nozzle was attached to a robot (HP-20, Motoman, Yaskawa Electric Corp., Waukegan, IL, USA) for control and repeatability of the coating deposition. A volumetric powder feeder (5MPE, SulzerMetco, Westbury, NY, USA) was used to transport the powder through the nozzle and increase the powder particle velocity. Argon was used as the carrier gas for the powder feeder, which was fed into the cold spray system at a pressure of 414 kPa gage (60 psig) and at a flow rate of 6 m^3/h (20 standard cubic feet per hour). The powder was fed at a rate of 60 flow meter reading (FMR). The temperature and pressure of the compressed air in the cold spray nozzle was kept constant at 375 °C and 634 kPa gage (92 psig), respectively. The stand-off distance (S.O.D.) between the torch and substrate was 5 mm, with the torch traversing horizontally across the substrate at 5 mm/s. The substrate used was 3.175 mm thick 6061 Al alloy that was roughened with #24 alumina grit medium (Manus Abrasive Systems, Inc., Edmonton, AB, Canada) to promote adhesion of the coating. In order to ensure maximum alumina content in the MMC coating during friction stir processing (FSP), the coatings were deposited with widths between 12 and 16 mm. To accomplish this, the cold spray nozzle was set to increment at 3 mm after each deposition pass for four passes. The coating thickness was up to 1 mm.

After deposition and during FSP, the aluminum plates were secured to a table that traversed at a constant rate of 88 mm/min underneath a 12 mm diameter cylindrical FSP tool that had a smooth flat surface. The tool was attached to a milling machine (Model 786 × 2, Induma, Milano, Italy) and inclined with a 3° lead angle towards the direction of travel. The tool was plunged into the sample such that the entire surface was in contact with the coating. FSP was conducted at tool rotation speeds of 894 and 1723 rotations per minute (RPM). The plunge depth of the tool into the coating was proportional to the axial force measured with a six-axis load cell (JR3, Model 75E20S4, Woodland, CA, USA). The plunge depth was varied at the beginning of processing until the axial force was stabilized, and the average was force output was monitored.

A micro-Vickers hardness indenter (MVK-H1, Mitutoyo, Aurora, IL, USA) was used to measure the hardness of the as-sprayed and friction stir-processed coatings. Hardness measurements were made as per ASTM E384 [23] with indentations being spaced at least four diagonals apart as per ASTM C1327 [24]. A 15 s dwell time was applied. A 200 g force (gf) load was used during indentation of the cross-section of the as-sprayed coatings and a 300 gf load was used on the cross-sections of the friction stir-processed coatings in order to produce larger indents on the harder material. Microhardness indents were made on the cross-section of the as-sprayed coatings at varying distances from the substrate. Indents were made at 20%, 40%, 60%, and 80% of the total coating thickness, with a minimum of 50 indents ($n \geq 50$) being taken. This provided an average representation of the hardness throughout the entire coating. Due to the triangular shape of the as-sprayed coating cross-section, the number of indents near the top of the coating was fewer than those taken near the substrate. A minimum of 15 indents ($n \geq 15$) were taken on each sample after FSP.

A scanning electron microscope (EVOMA15, Zeiss, Cambridge, UK), equipped with a energy-dispersive X-ray spectroscopy (EDX), was used to capture images of the MMC coatings to facilitate their

characterization. Image analysis software (Adobe Photoshop CS3, San Jose, CA, USA) was used to quantify the Al_2O_3 content before and after FSP. At least three images were taken of each sample, with at least four random sections of each image analyzed to determine the Al_2O_3 content. This provided an average volume percent (vol.%) of Al_2O_3 in each coating, which was then converted to weight percent (wt.%) based on the density values of Al and Al_2O_3 being 2.7 and 4.0 g/cm^3, respectively [25].

3. Results and discussion

The present study has focused on the fabrication of a coating with improved material properties after cold spraying with low pressure, followed by friction stir processing. Fig. 1 shows a magnified cross-section of a 100 wt.% Al coating, with the presence of pores that have formed during the cold spray process. Due to the high velocities (order of 500 m/s) achieved during cold spraying using this system, the Al particles deform plastically on impact. EDX was used to verify all areas in the coating in Fig. 1 as pure Al. The low density and irregular particle morphology of the Al particles may have promoted the formation of pores as gas was entrapped in the coating during the deposition process, as the level of porosity was lower when elliptical particles were employed [5]. SEM images of the powders used in this study are shown in Fig. 2. Many efforts have been made to reduce the formation of pores in cold-sprayed coatings due to their adverse effect on mechanical properties [8,10,26,27].

Figs. 3 and 4 show magnified cross-sections of MMC coatings deposited using feed powder containing 25 wt.% and 90 wt.% Al_2O_3, which resulted in coatings containing 17 wt.% and 48 wt.% Al_2O_3, respectively (Fig. 5). As the Al_2O_3 content of the feed powder was increased, agglomeration of this reinforcing phase between the boundaries of the initial Al particles increased, leaving the Al metal matrix devoid of particle reinforcement. EDX was used to verify that the black areas in Fig. 3 were Al_2O_3, bearing in mind that these reinforcing particles could be removed during polishing to leave behind voids. Direct quantification of the coating porosity from Figs. 3 and 4 with the imaging software was difficult due to the low contrast of Al_2O_3 particles versus pores. Instead, the regions of Al_2O_3 particles were individually isolated at higher magnification, and quantified as a volume fraction, which was converted to a weight fraction. Fig. 5 shows a plot of the weight fraction of Al_2O_3 particles in the MMC coating as a function of the weight fraction of Al_2O_3 in the feed powder. The results indicate that the content of Al_2O_3 increases in the

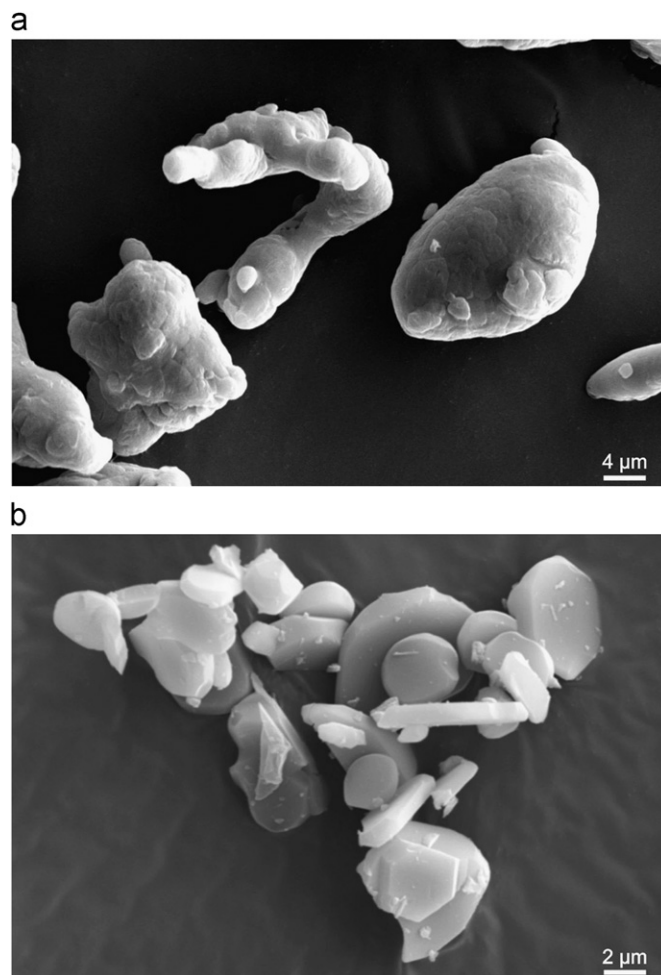**Fig. 2.** SEM micrographs of (a) $-45\ \mu m$ Al powder and (b) 10 μm Al_2O_3 powder.

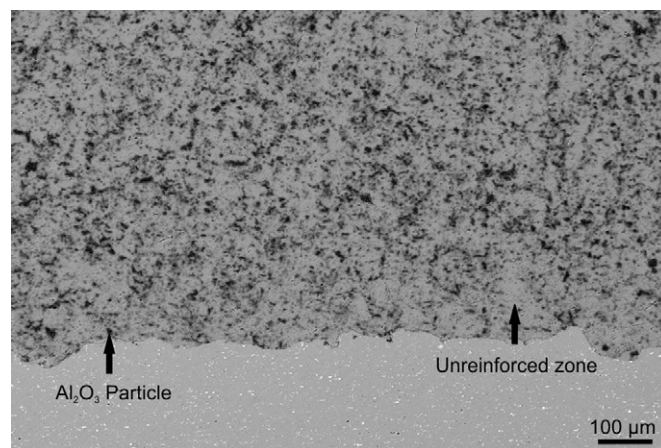**Fig. 3.** SEM micrograph of a cold-sprayed coating fabricated from Al–25 wt.% Al_2O_3 powder blend.

coating as the content of Al_2O_3 in the feed powder increases. Irissou et al. [10] have shown that as the content of Al_2O_3 in the feed powder increases, the Al_2O_3 content in the coating stabilizes at about 25 wt.%. However, in this study, the Al_2O_3 content in the MMC coating was 48 wt.% when 90 wt.% Al_2O_3 was included in the feed powder. The improvement in Al_2O_3 content may be due to the use of smaller Al_2O_3 powder particles and Al feed powder with an irregular morphology. The Al powder used by Irissou et al. [10] contained
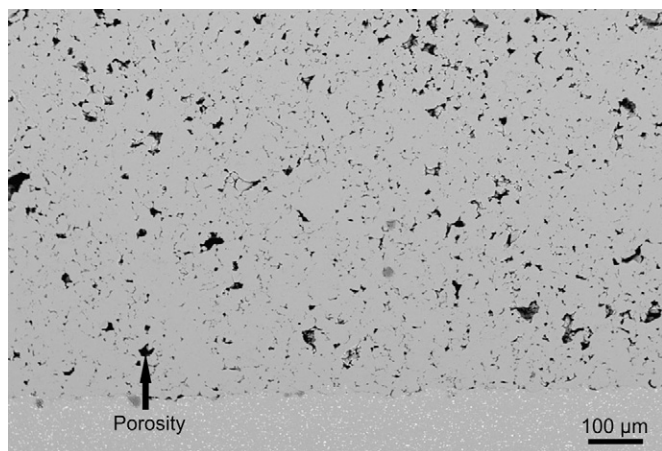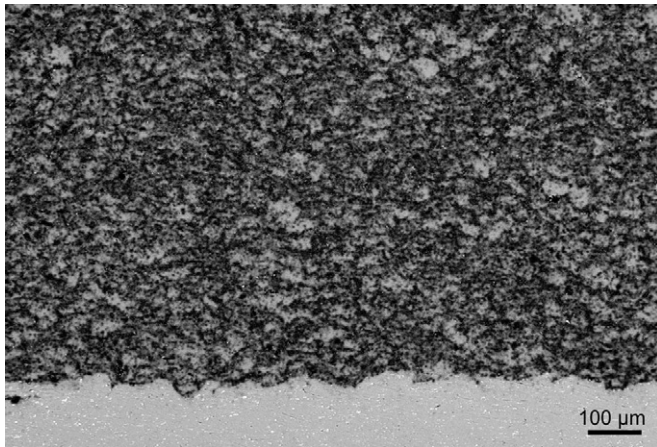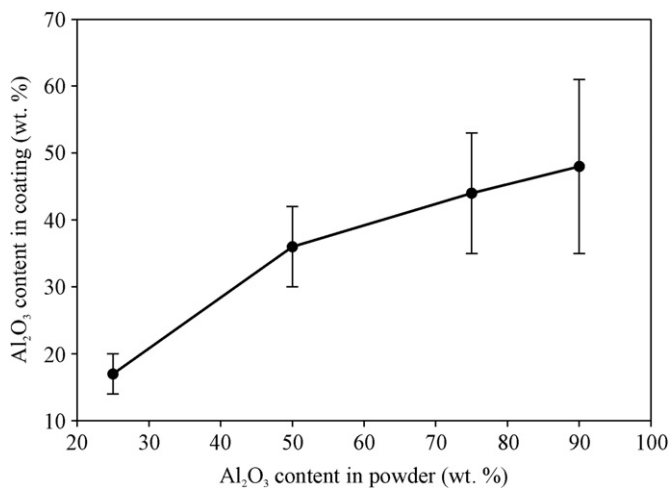

Fig. 1. SEM micrograph of a cold-sprayed coating fabricated from 100 wt.% Al feed powder.

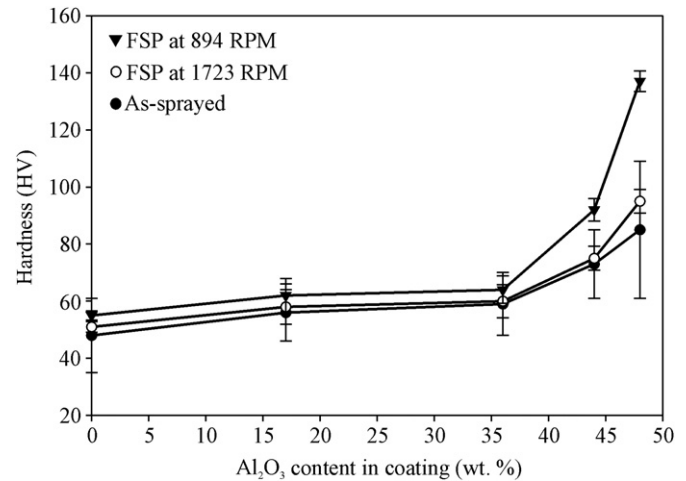Fig. 4. SEM micrograph of a cold-sprayed coating fabricated from Al–90 wt.% Al$_2$O$_3$ powder blend.

Fig. 6. Plot of MMC coating hardness as a function of Al$_2$O$_3$ content.

Fig. 5. Plot of Al$_2$O$_3$ weight fraction in the MMC coating as a function of Al$_2$O$_3$ weight fraction in the cold-sprayed feed powder blend.

large ($d_m = 81.5\,\mu$m), spherical particles, which may have been more difficult to deposit.

It has been shown by Irissou et al. [10] that increasing the weight fraction of the reinforcing phase in the cold spray feed powder can cause a decrease in deposition efficiency, which is defined as the ratio of powder in the coating compared to the amount of powder successfully deposited as a coating. Fig. 5 also suggests that an increase in the weight fraction of Al$_2$O$_3$ in the feed powder resulted in a decrease in the deposition efficiency. Spencer et al. [9] have hypothesized that the decrease in deposition efficiency in the MMC coating with increasing weight fraction of Al$_2$O$_3$ in the feed powder is caused by in-flight particle interaction and rebounding of ceramic particles from the substrate. Rebounding of ceramic particles from the substrate occurs due to the inability of Al$_2$O$_3$ particles to deform plastically under an applied force. Increasing the weight fraction of Al$_2$O$_3$ in the feed powder provides greater opportunity for particles to deflect, rather than adhere to the substrate, resulting in a decrease in deposition efficiency. However, regardless of the decrease in deposition efficiency, the amount of Al$_2$O$_3$ in the MMC coating increases due to the increase of Al$_2$O$_3$ in the feed powder.

Microhardness measurements were conducted on the as-sprayed coatings with Al$_2$O$_3$ weight fractions up to 48 wt.% (see Fig. 6). The non-uniform distribution of particles resulted in the wide scatter observed in the microhardness measurement values.

Since a low load (200 gf) was used, the indentations were often located exclusively in either the Al matrix material that was devoid of reinforcement, or in concentrated agglomerations of reinforcing particles, leading to the wide scatter. This was most obvious for the coatings with the highest fraction of Al$_2$O$_3$ particles. Fig. 6 shows that the average MMC coating hardness increases with Al$_2$O$_3$ weight fraction. For comparison, the hardness of the 100 wt.% Al powder coating was found to be 45 $\pm$ 8 HV ($n=50$). In the present study, when the as-deposited coating contained 17 wt.% Al$_2$O$_3$ the hardness increased to 57 $\pm$ 10 HV ($n=50$), which represented a 27% increase. However, the greatest efficiency in strengthening was observed when the coating contained fractions of Al$_2$O$_3$ above 36 wt.%. For example, when 48 wt.% Al$_2$O$_3$ was present in the MMC coating (Fig. 5) the hardness increased to 85 $\pm$ 24 HV ($n=50$). The heterogeneous distribution of the reinforcing particles in the MMC matrix resulted in a large standard deviation in the average hardness measurements.

The cold-sprayed coatings shown in Figs. 1, 3 and 4 were exposed to FSP at rotation speeds of 894 and 1723 RPM. The cold-sprayed MMC coating containing 48 wt.% Al$_2$O$_3$ exhibited the largest increase in hardness after exposure to FSP at 894 RPM, reaching a maximum of 137 $\pm$ 9 HV ($n=25$), which was higher than that of the base 6061 Al substrate (105 $\pm$ 3 HV ($n=15$)). The hardness values of each coating sample remained constant at varying distances from the substrate, suggesting that reinforcement was homogenous in the cold-sprayed MMC coatings after FSP. This is supported by the small error bars shown in Fig. 6, particularly for the coatings that were friction stir processed at 894 RPM. The hardness values of the MMC coatings exposed to FSP using a tool rotation speed of 1723 RPM were inferior to those of the coatings exposed at the lower rotation speed.

The large difference in hardness between the cold-sprayed coating of 100 wt.% Al powder (45 HV) and the base 6061 Al substrate (105 HV) is partly due to the presence of pores in the coating, as well as the precipitate particles in the Al 6061 substrate in the peak-aged condition. Dramatic increases in hardness have been shown in composites reinforced by ceramic particles, where the values of over 100 HV have been reported for cold-sprayed Al–Al$_2$O$_3$ MMC coatings [10] due to the presence of higher fractions of reinforcing Al$_2$O$_3$ particles. The rule of mixtures was used to compare the experimental hardness values of the MMC coatings to expected theoretical values. In the case where the hardness of the reinforcing phase is much higher than that of the matrix, and the volume fraction of the matrix is larger than the reinforcing phase, then the rule of mixtures suggest that

the lower limit of the hardness of the composite, H_c, will be given by:

$$H_c = \frac{H_p H_m}{f_m H_p + f_p H_m}, \tag{1}$$

where H_p and H_m are the hardness values of the reinforcing particles and matrix, respectively, while f_p and f_m are the volume fractions of the particles and the matrix, respectively. This has been shown to be valid for friction stir-processed Mg–Al$_2$O$_3$ metal matrix composites [28] and Mg–SiO$_2$ and Mg–ZrO$_2$ nanoparticle metal matrix composites [29].

The particle and matrix hardness values are 1365 HV for Al$_2$O$_3$ [25] and 45 HV for 100 wt.% Al coating. By using Eq. (3), a theoretical hardness value of 68 HV was calculated for an MMC coating consisting of an Al matrix reinforced with 36 vol.% (44 wt.%) Al$_2$O$_3$. This calculated hardness is close to the value measured for as-sprayed and friction stir-processed coatings at 1723 RPM (see Fig. 6). The increased hardness of the composite coatings processed at a lower rotation speed of 894 RPM is argued to be primarily a result of the improved distribution of particles, and likely also enhanced by the mechanical deformation and grain refinement of the aluminum matrix, which has been widely shown to increase when the tool rotation speed is reduced during friction stir processing [30–36].

The increased hardness of the cold-sprayed MMC coating observed with higher Al$_2$O$_3$ weight fractions in the feed powder may also be related to enhanced particle fracture upon deposition. For example, it is expected that during cold spray deposition, softer Al particles deform into splats, while some of the ceramic Al$_2$O$_3$ particles fracture. When the Al$_2$O$_3$ weight fraction of the feed powder is below 50 wt.%, there are a sufficient number of larger Al particles to deform plastically around the smaller ceramic particles. However, when the ratio of ceramic to metal particles is increased, the amount of Al$_2$O$_3$ particles that impact the substrate is higher. The increased rate at which Al$_2$O$_3$ particles interact with the surface may allow for more Al$_2$O$_3$ particles to fracture within the MMC matrix. Table 1 shows the average particle size of the reinforcing Al$_2$O$_3$ in the as-sprayed cold-sprayed MMC coatings deposited using feed powder that contained between 25 and 90 wt.% Al$_2$O$_3$. At least three SEM micrographs of each feed powder composition were used for the calculations, with at least fifty particles measured per micrograph. There is a clear change in the Al$_2$O$_3$ size distribution towards smaller diameter particles as the weight fraction of Al$_2$O$_3$ in the feed powder increases. The decrease in the average Al$_2$O$_3$ particle size in the MMC coatings observed with increased Al$_2$O$_3$ weight also suggests that fracture of these particles occurred during impact. This is due to the increased probability of impact between in-flight Al$_2$O$_3$ particles, as well as with the previously deposited Al$_2$O$_3$ particles lodged in the MMC coating. In particular, an Al–Al$_2$O$_3$ MMC coating deposited using 25 wt.% Al$_2$O$_3$ in the feed powder (17 wt.% Al$_2$O$_3$ in the coating) had an average particle size of $8 \pm 3.6 \, \mu m^2$ ($n = 100$), while a MMC
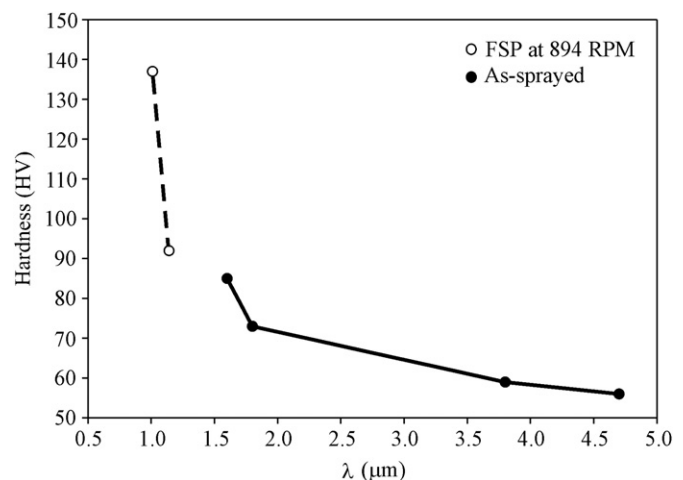
coating fabricated from a feed powder blend containing 90 wt.% Al$_2$O$_3$ (48 wt.% Al$_2$O$_3$ in the coating) had an average particle size of $4 \pm 1.7 \, \mu m^2$ ($n = 100$). This decrease in the average particle size may also have an influence on the coating properties. Fracturing of Al$_2$O$_3$ particles results in the coupled effect of introducing smaller reinforcing particles in the matrix and decreasing the distance between adjacent particles, and this aspect needs to be considered further.

The decrease in the particle size results in a corresponding decrease in the distances between adjacent particles or a decrease in the inter-particle mean free path. Kouzeli et al. [37] have used inter-particle mean free path to explain hardness improvements of MMC coatings due to particle reinforcement. As the Al$_2$O$_3$ content in the coating increases, the space between adjacent particles decreases. It has been shown that mean free inter-particle distances below 10 μm have a significant effect on MMC coating hardness [37]. The mean free inter-particle distance, λ, can be calculated by using

$$\lambda = \frac{1 - f_m}{N_L}, \tag{2}$$

where f_m is the volume fraction of particles and N_L is the number of particle intercepts per unit length test line [37]. λ was calculated and plotted as a function of hardness of the Al–Al$_2$O$_3$ MMC coatings, which is shown in Fig. 7. The figure agrees well with the previous hypothesis, and a distinct increase in hardness is observed when the values of λ below 5 μm are achieved in the as-sprayed coating, or when λ values around 1 μm are obtained after FSP. These results suggest that the reduction in mean free inter-particle distance of the Al$_2$O$_3$ reinforcing particles contributed to the observed increase in hardness in the MMC cold-sprayed coatings.

It is possible that refinement of the Al matrix during deposition of the feed powder blend may have also contributed to the improvements in hardness observed in Fig. 6. Cold spray deposition has been shown to work-harden the previously deposited coating layers, resulting in increased hardness during MMC coating fabrication [38,39]. Work hardening increases the hardness of MMC coatings by promoting grain refinement within the matrix, and it has already been shown that significant grain refinement occurs when pure Al is deposited via cold spraying [5]. One would expect the finer grain structures and further work hardening of the matrix to occur when Al$_2$O$_3$ particles are added to the feedstock stream, due to the shot-peening effects imparted by these particles when they do not adhere to the substrate.

Table 1
Average Al$_2$O$_3$ particle sizes in the Al–Al$_2$O$_3$ MMC coatings.

Al$_2$O$_3$ content in coating (wt.%)	Particle size (μm^2)
17	8 ± 3.6
36	6 ± 3.1
44	5 ± 2.1
48	4 ± 1.7
48[a]	2 ± 0.9

[a] After FSP at 894 RPM.

Fig. 7. Plot of MMC coating hardness as a function of inter-particle mean free path (λ).

Admixing Al and Al_2O_3 feed powders to facilitate deposition of MMC coatings clearly increased hardness by decreasing the mean free inter-particle distances between the reinforcing particles. Although the coating hardness was improved by the introduction of Al_2O_3 particles, another objective of this study was to determine the feasibility of coupling cold spraying at low pressure with FSP. Based on Fig. 6, performing FSP on a MMC coating that contains 48 wt.% Al_2O_3 resulted in the highest hardness of 137 ± 9 HV ($n=25$), which represents an increase of 30% when compared to the Al 6061 substrate. Fig. 8 shows a higher magnification cross-section of the MMC coating that contains 48 wt.% Al_2O_3 that has undergone FSP at 894 RPM. The FSP tool was plunged into the coating region, and the interface with the substrate has been disrupted. The Al matrix regions no longer contain agglomerations of reinforcing particles as shown in Figs. 3 and 4. This indicates that FSP has successfully re-distributed the reinforcing particles by plastically deforming the MMC coating matrix further leading to a more homogeneous coating structure. A schematic that depicts how the reinforcing particles are re-distributed during FSP is shown in Fig. 9. The re-distribution caused by the FSP procedure allows for greater uniform load sharing between the reinforcing Al_2O_3 particles during hardness indentation. In addition to re-distribution, FSP has also succeeded in further decreasing the size distribution of the Al_2O_3 particles. The average Al_2O_3 particle size decreased to 2 ± 0.89 μm^2 ($n=100$) for the MMC coating containing 48 wt.% Al_2O_3. The Al_2O_3 weight fraction in the coating did not change as a result of FSP, suggesting that mass loss did not occur due to the process.
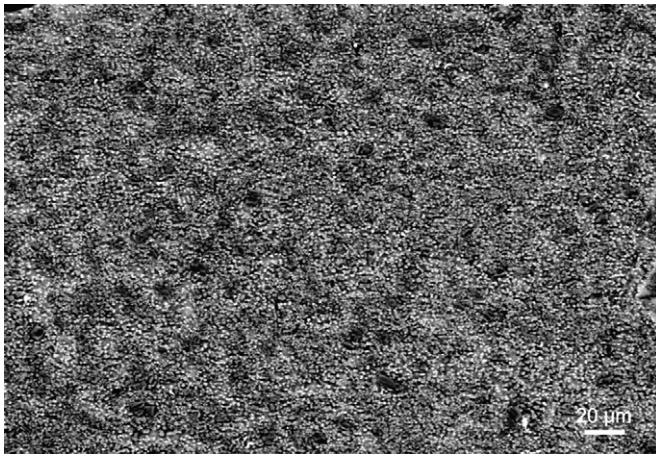
As such, particle fracture lead to a decrease in particle size accounting for the decrease in the measured particle mean free path, λ, after FSP. It has already been shown that λ values below 10 μm significantly improve hardness [37], while the values of around 1 μm were achieved after FSP in this present study (see Fig. 7). This may explain why the hardness values of the friction stir-processed coatings exceeded that of the substrate as well as the as-sprayed MMC coating (see Fig. 6).

The mechanical properties of MMC materials are governed by the mean free path between the particles. Uniform inter-particle spacing promoted by conducting FSP can improve the yield strength of the coating, as well as the hardness. Gustafson et al. [40] and Lee et al. [41] have reported a linear increase in the yield strength as a function of $1/\sqrt{\lambda}$ for particle-reinforced composites. The hardness as a function of the inverse square root of the mean free inter-particle distance is shown in Fig. 10 for the samples produced in this study. The figure shows a nearly linear relationship between the hardness of the as-sprayed MMC coating and $1/\sqrt{\lambda}$. The deviation of the data point corresponding to the coating that contains 48 wt.% Al_2O_3 that was exposed to FSP at 894 RPM may be due to the Al_2O_3 weight fraction in the coating being higher than the 48 wt.% that was calculated. This can be correlated with Fig. 5 where a large deviation can be seen with cold-sprayed MMC coatings deposited using a 90 wt.% Al_2O_3 feed powder. It should be noted that an empirical correlation between hardness and three times the yield strength has been observed for many alloys [42,43], and this is also suggested from an initial
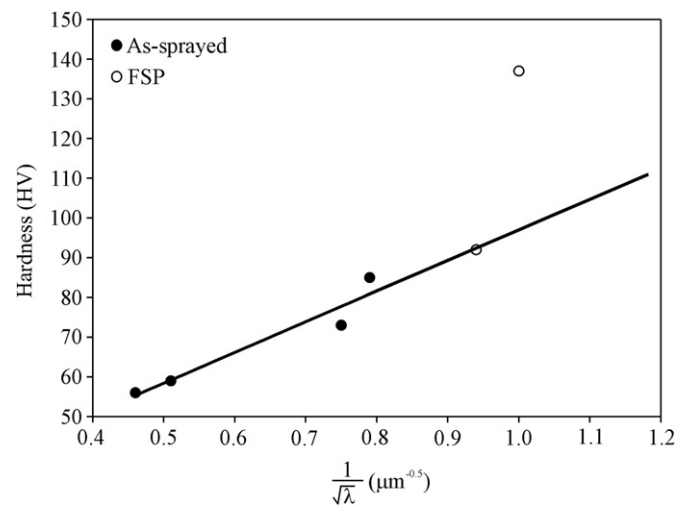

Fig. 8. SEM micrograph of a cold-sprayed coating fabricated from Al–90 wt.% Al_2O_3 powder blend after FSP at 894 RPM.

Fig. 10. MMC coating hardness as a function of the inverse square root of the mean free inter-particle distance (λ).
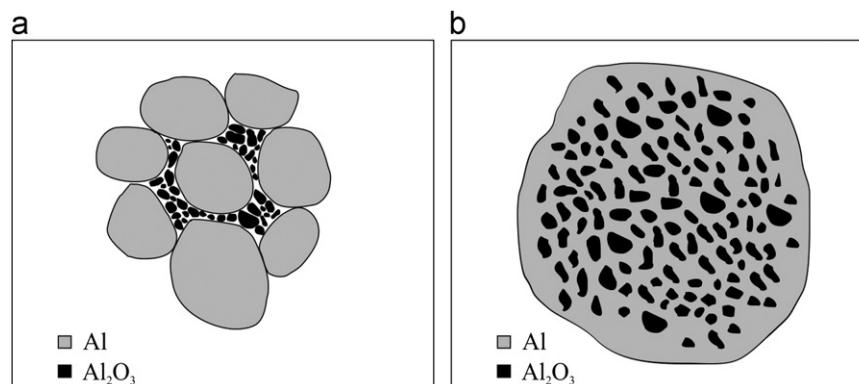

Fig. 9. Schematic of reinforcing particle re-distribution in MMC coatings during FSP.

analysis proposed by Bishop et al. [44]. Although this correlation is quite accurate for ferritic steels and bulk metallic glasses, depending on the ductility of the metal, the correlation coefficient may range from 2.3 to 3.7 [45].

The linear relationship between yield strength or hardness and $1/\sqrt{\lambda}$ may be justified by considering the concept of geometrically and statistically stored dislocations [40,41]. Uniform deformation in a material leads to an increase in the density of dislocations, and these dislocations are statistically stored dislocations. Non-uniform deformation leads to the formation of geometrically stored dislocations. When a metal matrix composite experiences deformation, strain localization in the matrix, coupled with the difference between the mechanical behavior of the matrix and the reinforcing material, leads to the generation of both statistical and geometrical dislocations [46], and these sources both contribute to strain hardening. In addition, the stress gradient between the relatively soft matrix and hard reinforcing particles can also be considered as a strengthening factor. All these mechanisms are directly dependent to the mean free inter-particle spacing, and a shorter spacing creates increased barriers to dislocation motion which will increase the work hardening rate [47].

Interestingly, Fig. 10 also shows that the hardness versus inter-particle spacing of the composite following FSP using 894 RPM drastically deviates from the trend established for the as-sprayed MMC coatings. This suggests that the application of FSP enhances the hardness not only by reducing the inter-particle spacing, but perhaps by other mechanisms. For example, a significant temperature rise occurs during FSP which usually reaches as high as 90% of the incipient melting point of the matrix alloy [48,49], and the consequent cooling can lead to an increase in the density of geometrically stored dislocations that are generated to accommodate the deformation caused by the mismatch in coefficient of thermal expansion between the matrix and the particles [37]. It is well known that grain refinement occurs during FSP as a result of dynamic recrystallization [17,18], typically resulting in grain sizes that are $< 10 \, \mu m$, and even finer when there are ceramic reinforcing particles present with sizes $< 1 \, \mu m$ [50] due to the suppression of grain growth by particle drag. This drastic reduction in the grain size during FSP is particularly significant when lower tool rotation speeds are applied [30–36]. This is an important point, considering that relationship between λ and hardness developed by Gustafson et al. [40] considered composites in which the grain size was larger than the inter-particle spacing. In that study, it was found that the metal between the reinforcing phase can essentially be treated as a single crystal with no grain boundary strengthening, and so the present deviation from the correlation between λ and hardness is likely due in part to grain refinement.

Samples of the cold-sprayed MMC coatings that were exposed to FSP at a tool rotation speed of 1723 RPM did not have a completely uniform particle distribution as shown in Fig. 11. Although the reinforcing particles have been more homogeneously re-distributed compared to the as-sprayed MMC coatings, sections of Al matrix devoid of Al_2O_3 particles are present. This contrasts the images presented in Fig. 8 of the MMC coatings after exposure to FSP at tool speeds of 894 RPM. It has been suggested earlier that the mean free inter-particle distance is the main mechanism for hardness increases in the MMC coatings. The coating fabricated from 90 wt.% Al_2O_3 feed powder (48 wt.% Al_2O_3 in the coating) exposed to FSP at 894 RPM possessed λ of $1.01 \pm 0.13 \, \mu m$ (see Fig. 7), while the same coating friction stir-processed at 1723 RPM had a λ of $2.1 \pm 0.40 \, \mu m$. This may explain the lower hardness (95 versus 137 HV) in the coating that was friction stir-processed at 1723 RPM compared to that processed at 894 RPM. It is suggested that the decrease in hardness due to the
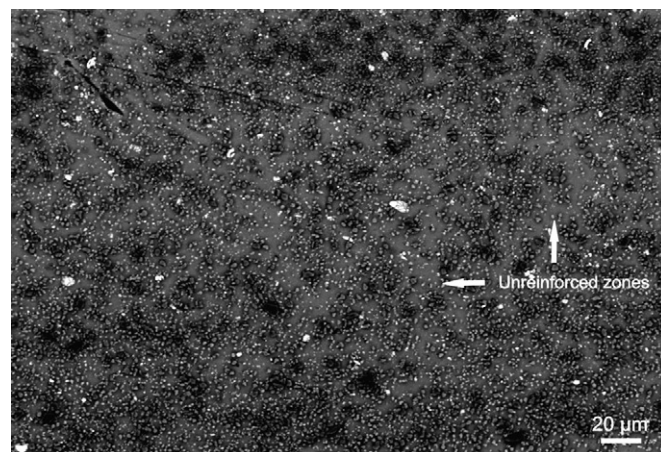

Fig. 11. SEM micrograph of a cold-sprayed coating fabricated from Al–90 wt.% Al_2O_3 powder blend after FSP at 1723 RPM.

faster rotation speed in FSP (1723 RPM) may be related to the incorporation of additional Al from the substrate into the matrix of the coating. The additional heat caused by the increased frictional force of the tool created a larger stir zone that incorporated the underlying Al substrate. It has been shown in prior work that the layer of stirred material is at least $100 \, \mu m$ thick beneath the bottom of a 4 mm diameter friction stir processing tool [51] and the use of a 12 mm diameter tool may lead to the formation of a stirred region that exceeded the thickness of the as-sprayed coating. When this occurs, the previously unaffected substrate is pulled into the coating during processing, increasing the quantity of Al present in the processed coating to produce a structure with regions devoid of reinforcement as shown in Fig. 11. This effect would be beneficial if the Al matrix incorporated into the MMC retained its original hardness. However, FSP of heat treated Al alloy is known to have decreased the hardness of the alloy due to heating above the solvus temperature of the precipitates [52]. This effect may increase the inter-particle distance of the reinforcing particles, decreasing the overall average hardness of the cold-sprayed MMC coating.

4. Conclusion

An investigation of particle reinforcement within cold-sprayed MMC coatings and the feasibility of coupling low-pressure cold spraying with FSP were conducted. An analysis of the microstructures of the cold-sprayed MMC coatings determined that the mean free inter-particle distance (λ) of Al_2O_3 particles in the MMC coatings may be the main mechanism contributing to increased hardness. SEM micrographs confirmed that 90 wt.% Al_2O_3 admixed with Al feed powder during cold spraying was successful to achieve mean free particle distances, $\lambda \leq 10 \, \mu m$, providing an increase in hardness of 77% when compared to a commercially pure Al powder-based coating. The decreased λ values were possible due to the decreased size distribution determined from image analysis.

The highest volume fraction of Al_2O_3 which could be obtained in the MMC was 48 wt.% when a feedstock of 90 wt.% Al_2O_3 was used during cold spraying. The hardness of this coating increased from 85 HV to a maximum observed hardness of 137 HV when friction stir processing was performed using a tool rotation speed of 894 RPM. Analysis of micrographs of the cold-sprayed MMC coatings after FSP indicated that the hardness increase was possible due to the successful re-distribution of the Al_2O_3 particles trapped within the grain boundaries of the Al matrix.

This re-distribution resulted in particle mean free path distances of $\lambda \le 5 \mu m$, allowing for increased load sharing and increased hardness values. When the FSP tool rotation speed was increased to 1723 RPM, this enabled Al 6061 alloy base material to be incorporated into the Al matrix, which produced higher particle mean free path values of λ and reduced the hardness of the MMC coating. These results suggest that coupling cold spraying with FSP improves the hardness of Al–Al$_2$O$_3$ composites and provides a reliable method to fabricate dense MMC coatings with improved material properties compared to the original substrate.

Acknowledgements

References

[1] A. Papyrin, Adv. Mater. Process 159 (2001) 49–51.
[2] S. Klinkov, V. Kosarev, M. Rein, Aero. Sci. Technol. 9 (2005) 582–591.
[3] M. Grujicic, in: V.K. Champagne (Ed.), Fundamentals of Cold-Gas Dynamic Spray, Woodhead Publishing Limited, London, 2007.
[4] H. Assadi, F. Gartner, T. Stoltenhoff, H. Kreye, Acta Mater. 51 (2003) 4379–4394.
[5] M. Dewar, A. McDonald, A. Gerlich, J. Mater. Sci. 47 (2012) 184–198.
[6] A. Portinha, V. Teixeira, J. Carneiro, J. Martins, M. Costa, R. Vassen, D. Stoever, Surf. Coat. Technol. 195 (2005) 245–251.
[7] X. Zhang, B. Xu, Y. Xu, F. Xuan, S. Tu, Appl. Surf. Sci. 254 (2008) 3879–3889.
[8] D. Poirier, J. Legoux, R. Drew, R. Gauvin, J. Therm. Spray Technol. 20 (2011) 275–284.
[9] K. Spencer, D. Fabijanic, M. Zhang, Surf. Coat. Technol. 204 (2009) 336–344.
[10] E. Irissou, J. Legoux, B. Arsenault, C. Moreau, J. Therm. Spray Technol. 16 (2007) 661–668.
[11] R. Lima, J. Karthikeyan, C. Kay, J. Lindemann, C. Berndt, Thin Solid Films 416 (2002) 129–135.
[12] H. Kim, C. Lee, S. Hwang, Surf. Coat. Technol. 191 (2005) 335–340.
[13] H. Lee, H. Shin, K. Ko, J. Therm. Spray Technol. 102 (2010) 102–110.
[14] Y. Morisada, H. Fujii, T. Mizuno, G. Abe, T. Nagaoka, M. Fukusumi, Surf. Coat. Technol. 204 (2010) 2459–2464.
[15] R. Mishra, Z. Ma, I. Charit, Mater. Sci. Eng. A 341 (2003) 307–310.
[16] B. Zahmatkesh, M. Enayati, Mater. Sci. Eng. A 527 (2010) 6734–6740.
[17] S. Mousavizade, F. Malek Ghaini, M. Torkamny, J. Sabbaghzadeh, A. Abdollah-zadeh, Scripta Mater. 60 (2009) 244–247.
[18] Z. Ma, Metall. Mater. Trans. A 39A (2008) 642–658.
[19] A. Kurt, I. Uygur, E. Cete, J. Mater. Process. Technol. 211 (2011) 313–317.
[20] A. Feng, B. Xiao, Z. Ma, Compos. Sci. Technol. 68 (2008) 2141–2148.
[21] A. Pirondi, L. Collini, Int. J. Fatigue 31 (2009) 111–121.
[22] J. Karthikeyan, Adv. Mater. Process 163 (2005) 33–35.
[23] ASTM E384-11, Standard Test Method for Knoop and Vickers Hardness of Materials, ASTM International, West Conshohocken, PA, 2011.
[24] ASTM C1327-08, Standard Test Method for Vickers Indentation Hardness of Advanced Ceramics, ASTM International, West Conshohocken, PA, 2008.
[25] W. Smith, J. Hashemi, Foundations of Materials Science and Engineering, fourth ed., McGraw-Hill Co., New York, 2006.
[26] D. Goldbaum, J. Ajaja, R. Chromik, W. Wong, S. Yue, E. Irissou, J. Legoux, Mater. Sci. Eng. A 530 (2011) 253–265.
[27] J. Ajaja, D. Goldbaum, R. Chromik, Acta Astron. 69 (2011) 923–928.
[28] M. Azizieh, A. Kokabi, P. Abachi, Mater. Des. 32 (2011) 2034–2041.
[29] C. Chang, Y. Wang, H. Pei, C. Lee, J. Huang, Mater. Trans. 47 (2006) 2942–2949.
[30] A. Hassan, P. Prangnell, A. Norman, D. Price, S. Williams, Sci. Technol. Weld. Join. 8 (2003) 257–268.
[31] A. Hassan, A. Norman, D. Price, P. Prangnell, Acta Mater. 51 (2003) 1923–1936.
[32] R. Mishra, Z. Ma, Mater. Sci. Eng. R 50 (2005) 1–78.
[33] C. Chang, C. Lee, J. Huang, Scripta Mater. 51 (2004) 509–514.
[34] T. Hirata, T. Oguri, H. Hagino, T. Tanaka, S.W. Chung, Y. Takigawa, K. Higashi, Mater. Sci. Eng. A 456 (2007) 344–349.
[35] T. Shibayanagi, M. Naka, Mat. Sci. Forum 539–543 (2007) 3769–3774.
[36] Y.S. Sato, M. Urata, H. Kokawa, Metall. Mater. Trans. A 33 (2002) 625–635.
[37] M. Kouzeli, A. Mortensen, Acta Mater. 50 (2002) 39–51.
[38] Y. Tao, T. Xiong, C. Sun, H. Jin, H. Du, T. Li, Appl. Surf. Sci. 256 (2009) 261–266.
[39] X. Luo, G. Yang, C. Li, Surf. Coat. Technol. 205 (2011) 4808–4813.
[40] T. Gustafson, P. Panda, G. Song, R. Raj, Acta Mater. 45 (1997) 1633–1643.
[41] I. Lee, C. Hsu, C. Chen, N. Ho, P. Kao, Compos. Sci. Technol. 71 (2011) 693–698.
[42] P. Sanders, C. Youngdahl, J. Weertman, Mater. Sci. Eng. A 234–236 (1997) 77–82.
[43] X. An, S. Wu, Z. Zhang, R. Figueiredo, N. Gao, T. Langdom, Scripta Mater. 63 (2010) 560–563.
[44] R. Bishop, R. Hill, N. Mott, Proc. Phys. Soc. 57 (1945) 147–159.
[45] P. Zhang, S. Li, Z. Zhang, Mater. Sci. Eng. A 529 (2011) 62–73.
[46] G. Dieter, Mechanical Metallurgy, third ed., McGraw-Hill Co., New York, 1986.
[47] D. McDanels, Metall. Trans. A 16A (1985) 1105–1115.
[48] P. Colegrove, H. Shercliff, Sci. Technol. Weld. Join. 8 (2003) 360–368.
[49] A. Gerlich, P. Su, T. North, Sci. Technol. Weld. Join. 10 (2005) 647–652.
[50] C. Lee, J. Huang, P. Hsieh, Scripta Mater. 54 (2006) 1415–1420.
[51] P. Su, A. Gerlich, T. North, G. Bendzsak, Sci. Technol. Weld. Join. 11 (2006) 61–71.
[52] Y. Sato, H. Kokawa, Metall. Mater. Trans. A 32 (2001) 3023–3031.